Atmospheric dynamics govern northern hemisphere wintertime climate variations forced by changes in earth's orbit

Alex Hall

Dep't of Atmospheric Sciences, University of California—Los Angeles, Los Angeles, CA 90095

Amy Clement

Rosenstiel School of Marine and Atmospheric Science, University of Miami, Miami, FL 33149

David W. J. Thompson

Dep't of Atmospheric Science, Colorado State University, Fort Collins, CO 80523

Anthony Broccoli

Department of Environmental Sciences, Rutgers University, New Brunswick, NJ 08901

Charles Jackson

Institute for Geophysics, The John A. and Katherine G. Jackson School of Geosciences, The University of Texas at Austin, Austin, Texas 78759-8500.

Corresponding author address. E-mail: alexhall@atmos.ucla.edu

ABSTRACT

Milankovitch proposed that variations in earth's orbit cause climate variability through a local thermodynamic response to changes in insolation. We test this by examining variability in an atmospheric general circulation model coupled to an ocean mixed layer model subjected to orbital forcing of the past 165,000 years. During northern hemisphere summer, the model's response conforms to Milankovitch's hypothesis, with high (low) insolation generating warm (cold) temperatures throughout the hemisphere. However, during northern hemisphere winter, the climate variations stemming from orbital forcing cannot be solely understood as a local thermodynamic response to radiation anomalies. Instead orbital forcing perturbs the atmospheric circulation in a pattern bearing a striking resemblance to the northern annular mode, the primary mode of simulated and observed unforced atmospheric variability. The hypothesized reason for this similarity is that the circulation response to orbital forcing reflects the same dynamics generating unforced variability. These circulation anomalies are in turn responsible for significant fluctuations in other climate variables: Most of the simulated orbital signatures in wintertime surface air temperature over mid-latitude continents are directly traceable not to local radiative forcing, but to orbital excitation of the northern annular mode. This has paleoclimate implications: During the point of the model integration corresponding to the last interglacial (Eemian) period, the orbital excitation of this mode generates a 1-2°C warm surface air temperature anomaly over Europe, providing an explanation for the warm anomaly of comparable magnitude implied by the paleoclimate proxy record. The results imply that interpretations of the paleoclimate record must account for changes in surface temperature driven not only by changes in insolation, but also by perturbations in atmospheric dynamics.

1. Introduction

Much of the internal variability of the present-day climate stems from well-known modes of climate variability. These modes are products of dynamical processes within the atmosphere-ocean system. Prominent among them are the El Niño/Southern Oscillation (ENSO) phenomenon in the tropics (Philander 1990), and the annular modes in the extratropics of the northern (e.g. Hurrell 1995, Thompson and Wallace 2000; Hurrell et al. 2003) and southern (e.g. Kidson 1988; Karoly 1990; Hartmann and Lo 1998; Thompson and Wallace 2000) hemispheres. Like ENSO, the northern annular mode (NAM, also known as the North Atlantic Oscillation and Arctic Oscillation) is linked with significant variability in temperature and other climate variables because of its association with atmospheric circulation anomalies (e.g. Hurrell et al. 2003). It would therefore alter surface climate if it were perturbed. The dynamical response of ENSO to orbital forcing has been proposed as an important component of paleoclimate variability (Clement et al. 1999). However, extratropical paleoclimate has not been viewed in terms of known modes of variability, and attention has commonly focused instead on the direct thermodynamic response to orbital forcing, particularly on how variations in boreal summer insolation can lead to an ice age (Hays et al. 1976; Imbrie et al. 1984). In this study, we demonstrate that the dynamics of the NAM are crucial to understanding the northern hemisphere (NH) extratropical wintertime response of a climate model to pure orbital forcing.

2. Experimental Design

The model we use to study this issue is an atmospheric general circulation model on a global domain coupled to mixed layer ocean model consisting of an isothermal 50 m depth slab. The model has a resolution of approximately 4.5° latitude by 7.5° longitude (see fig 2A for a view of the model's NH distribution of oceans and continents). There are nine vertical levels, with the top level coinciding roughly with a pressure of 25 hPa. As is standard practice when such a model configuration is employed, seasonal variations in deep ocean heat transport are included as a prescribed flux at the bottom of the ocean mixed layer. These heat fluxes are chosen to maintain present-day sea surface temperatures (SST) when the present-day orbital configuration is imposed. Sea ice dynamics and thermodynamics are included. A simple land surface model is employed, where surface temperatures are determined by heat balance assuming no storage of heat within the land. Soil moisture is predicted using a 15 cm depth bucket model formulation.

The variations in insolation associated with changes in earth's orbit of the past 165,000 years, taken from Berger (1992), are imposed on the model in a continuous fashion. We remind the reader briefly of the properties of this solar forcing. It results from variations in the obliquity of the earth's spin axis relative to the plane of the earth's orbit about the sun, precession of the earth's spin axis, and fluctuations in the eccentricity of the earth's orbit. Obliquity varies on a time scale of about 40,000 yrs. This changes the geographical distribution of insolation on both a seasonal and annual-mean basis. When obliquity is high, the summertime extratropics receive more sunshine, while less is

received elsewhere. The anomaly in the summertime extratropics is much larger than the anomaly elsewhere. On an annual-mean basis the tropics receive less sunshine when obliquity is high, while the high latitudes receive more. The earth's spin axis completes one precessional cycle in about 20,000 yrs. This cycle affects the time of year the earth comes closest to the sun (perihelion). The entire earth receives more sunshine at perihelion, so that the precessional forcing is in phase globally for any given time of year; however the anomaly is largest the lower the zenith angle. For example, if perihelion coincides with NH summer solstice, the insolation anomaly is larger in the NH. Unlike obliquity, precession does little to alter the geographical distribution of annual-mean insolation. Variations in eccentricity, occurring on approximately 100,000 yr time scales, also generate very little annual-mean signal. Their main effect is to modulate the strength of the precessional forcing.

The pace of the orbital variations of the past 165,000 yrs is accelerated by a factor of 30 in the simulation, so that the actual integration only lasts 5,500 yrs. The acceleration, which makes the experiment practical given limited computational resources, does not compromise our ability to diagnose the simulated response to orbital forcing, since the model equilibrates to the forcing within 10 model years. Even with the orbital variations taking place at the accelerated pace, this equilibration time is still approximately two orders of magnitude shorter than the time scale of the forcing's shortest periodicity. Since the experiment's goal is to isolate the effect of orbital forcing on climate variability, these are the only boundary conditions that change over the course of the integration. CO_2 and ozone, the only greenhouse gases in the model other than water

vapor, are fixed to present-day levels. The present-day configuration of continental ice

sheets is prescribed. The experiment therefore isolates the simulated response of the

atmosphere-ocean system to orbital forcing in the absence of variations stemming from

the historical growth and decay of the North American and Scandinavian ice sheets.

More detailed descriptions of the model and experimental design are provided in Jackson

and Broccoli (2003).

3. Analysis Techniques

In all raw model time series, both variability generated internally by the model and

fluctuations stemming from orbital forcing are noticeable. A typical example of this is

seen in fig 1A, which shows the simulated time series of SLP at a grid point near the

Azores in the central North Atlantic. Here pronounced variations in SLP on orbital times

scales are visible, as are higher-frequency fluctuations clearly unrelated to orbital forcing

and therefore generated by the model's internal dynamics. To separate the orbital and

internal variability, the raw time series are projected onto obliquity and precession basis

functions using a least-squares fitting procedure.   The time series of deviations of a given

climatic quantity from its mean value of the 165,000 yr simulation $X(t)$, is expressed as:

$$X(t) = A_o \Phi^{'}(t) + A_p e(t) \cos[\lambda(t) - \varphi_p] + R(t) \tag{1}$$

where t is time, $\Phi^{'}$ is the deviation of obliquity from its 165,000 yr mean, e is the

eccentricity, λ is the longitude of perihelion. The fitting procedure determines A_o, the

amplitude of the response that can be linearly related to obliquity forcing, as well as A_p,

the amplitude and φ_p, the phase of the response that can be linearly related to precessional

forcing. The residual $R(t)$ contains the remainder of the variability.

Lags in the atmosphere-ocean system could make a climate variable at any given time of year most sensitive to orbital insolation anomalies at an earlier time of year. For this reason we allow climate variables to have a phase as well as an amplitude relationship with the orbital forcing in eq. (1). The phase relationship is treated differently in the precession and obliquity cases. Precessional forcing has a phase relationship with the annual cycle that varies continuously through the ~20,000 yr precessional cycle. Therefore we allow the precession-related climate response to be anywhere from 0 to 360 degrees out of phase with the precessional forcing. A concrete instance of this, which we discuss later in this article, is the simulated response of SST to precessional forcing. Because of the ocean's thermal inertia, SST at any given time of year is generally most sensitive to solar forcing two to three months earlier. For example, the precession-related SST variations in January tend to reach their maximum value over much of the ocean when perihelion occurs in October, and so are in phase with the precessional variation of insolation in October. This information can be captured with an amplitude (A_p) and a phase (φ_p).

Obliquity forcing, unlike its precession counterpart, does not have a continuously varying phase relationship with the annual cycle. This is because obliquity-induced insolation anomalies throughout the calendar year are either in phase or out of phase with variations in the tilt of the earth's axis. An obliquity-related climate anomaly at any particular time of year may result from an instantaneous response to a simultaneous insolation anomaly or may instead stem from a sensitivity to obliquity forcing during another season. Either

7

way, it will be either in phase or out of phase with obliquity variations. This information

can be captured simply by allowing A_o to be either positive or negative. Our method of

extracting the simulated response to obliquity forcing is only appropriate for our

atmosphere-mixed layer ocean modeling framework, where the model equilibrates

quickly to changes in orbital configuration. If our atmospheric model were coupled

instead to a fully dynamical ocean model, response time lags of thousands of years could

occur in the deep ocean, and we would need to allow for a continuously varying phase

relationship with obliquity to capture this.

Figs 1b-e illustrate how the least-squares fitting procedure works for the Azores SLP time

series of fig 1A. Fig 1C shows $A_o\Phi'$(t), the variability in the time series that can be

linearly related to obliquity forcing.   Fig 1D shows $A_p e(t)\cos[\lambda(t)-\varphi_p]$, the variability

that can be linearly related to precessional forcing. The obliquity and precession

variations can be combined to give a time series of the total variability that can be

linearly related to orbital forcing, which we denote as "orbital" variability (fig 1B)

throughout this paper. A comparison of figs 1A and B reveals that the least-squares

fitting procedure works reasonably well; there is a clear correspondence, both in

amplitude and phase, between the orbital variability captured by the least-squares fitting

procedure and the orbital variations seen in the raw time series.

In principle, *R(t),* the variability remaining when the orbital variability is removed from

raw model time series includes three types of fluctuations: (1) internal variability, (2)

nonlinear response to orbital forcing, and (3) direct effects of the 100,000 year variations

in eccentricity. In practice, however, in most variables at most locations it is clear from visual inspection of $R(t)$ that internal variability overwhelmingly dominates over the two other types of fluctuations (e.g. fig 1E).   We therefore denote the residual remaining when orbital variability is removed from raw model time series as "internal" variability throughout this paper.

4. Annular Mode Response

The model's NH extratropical response to orbital forcing and its main modes of internal variability in this region can be summarized by an empirical orthogonal function (EOF) analysis of orbital and internal sea level pressure (SLP) variability (fig 2). We show results from both summer (JJA) and winter (DJF) seasons to highlight the dramatic difference in the simulated response to orbital forcing between these two seasons.

In summer, the signatures of local heating predominate in the primary pattern of the seasonal-mean SLP response to orbital forcing (fig 2A).   This pattern consists of anomalously low SLP over continents, and high SLP over oceans. The time series associated with it (black curve, fig 2B) is nearly perfectly correlated with a time series representing June NH extratropical orbital forcing (insolation anomalies at 40°N, orange curve, fig 2B). When the NH extratropics receive more summer insolation, the land areas warm more than the ocean because of smaller evaporative damping and effective heat capacity over land.   This causes a monsoon-like shift of atmospheric mass from the land to ocean.

If the main mode of orbital seasonal-mean SLP variations during winter could also be understood as a local thermodynamic response to orbital forcing, fig 2E would be similar to fig 2A with smaller amplitudes owing to the smaller size of the DJF insolation anomalies, and the time series associated with it would also be in phase with the forcing. Instead, fig 2E shows high SLP concentrated in two lobes over the mid latitude oceans and low SLP over the Arctic, and the associated time series is significantly out of phase with the time series representing December NH extratropical forcing (compare orange and black curves of fig 2F). These features are difficult to explain as a local thermodynamic response to orbital forcing.

The primary mode of orbital DJF SLP variability, shown in fig 2E, bears a striking resemblance to the primary mode of internal wintertime SLP variability, shown in fig 2G. With high pressure in two lobes associated with the NH Atlantic and Pacific storm tracks, and low pressure over the pole, this is the model's northern annular mode (NAM). The pattern is very similar to the real atmosphere's NAM (Thompson and Wallace 2000), despite the atmospheric model's coarse resolution. The NAM is hypothesized to dominate wintertime variability in both observations and models because of a positive feedback between mid-latitude westerlies and transient eddies in the NH storm tracks (Lorenz and Hartmann 2003). During the positive phase of the NAM, the extratropical eddies flux anomalously large amounts of westerly momentum across ~45°N (Limpasuvan and Hartmann 2000), giving rise to out-of-phase anomalies in the zonal wind between 30-35°N and 55-60°N. The anomalies in the zonal wind, in turn, organize

eddy activity such that the anomalies in the zonal flow are reinforced (Lorenz and

Hartmann 2003; Robinson 2000).

The relationship between zonal wind and the NAM is mirrored in the simulation, as seen

in the projection of the internal zonal-mean, zonal wind variability onto the primary mode

of internal SLP variability (fig 3B).   When orbital zonal winds are projected onto the

primary mode of orbital SLP variability (fig 3A), westerly anomalies centered near 55-

60°N and easterly anomalies centered near 30-35°N also result.   Thus both the horizontal

and vertical structures of the primary mode of orbital variability closely resemble those of

the NAM. This suggests the same eddy-mean flow interactions governing the primary

mode of internal wintertime circulation variability are also at play in selecting the

primary mode of orbital wintertime circulation variability. Though they reflect the same

fundamental phenomenon, we simplify the following discussion by denoting the mode

portrayed in fig 2E as the "orbital NAM", and the mode portrayed in fig G as the

"internal NAM". The NAM pattern does not dominate internal SLP variability in

summer (fig 2C), consistent with the dearth of eddy activity at this time of year.

A comparison of the SLP values shown in figs 2E and G indicates that the magnitudes of

the SLP anomalies associated with the orbital NAM are comparable to those associated

with the internal NAM. This is also suggested by visual inspection of the internal and

orbital components of the central North Atlantic SLP time series (shown in figs 1B and E

respectively).   This grid point is located in the N. Atlantic lobe of the NAM. The

11

internal and orbital fluctuations here, both of which are associated in large part with the NAM-like modes of variability of figs 2E and G, are comparable in magnitude.

5. The meridional SST gradient and the orbital NAM

Robinson (2000) and Kushnir et al. (2002) argue that changes in the meridional surface temperature gradient in middle latitudes can induce changes in the NAM via the relationship between lower tropospheric baroclinicity and the convergence of the eddy momentum flux in the upper troposphere. They theorize that along a latitude of enhanced meridional surface temperature gradient, there is increased generation of baroclinic eddies in the lower troposphere and thus increased convergence of the momentum flux in the upper troposphere as the eddies radiate away from their source latitude. The combined effects of the anomalous heat and momentum fluxes by the eddies give rise to equivalent barotropic westerly anomalies throughout the depth of the troposphere. Here we draw on this mechanism to argue that orbitally-induced variations in the wintertime extratropical meridional temperature gradient across the main axis of the westerly NAM anomalies near 55°N are very likely key to understanding why the model response to orbital forcing during NH winter is dominated by a pattern nearly identical to the NAM. For this reason we explain in this section how orbital variations in this temperature gradient arise in the simulation. We analyze the fluctuations stemming from obliquity and precessional forcing separately, since the mechanisms whereby the two types of forcing generate these fluctuations are different.

We focus first on obliquity. Fig 4A shows a Hovmuller diagram of the obliquity component of wintertime zonal-mean SST variability. A clear out-of-phase relationship is seen between SST poleward and equatorward of about 45°N. When obliquity is high, DJF SSTs fall below the mean in the tropics, and rise above the mean in high latitudes. This pattern reveals that the wintertime SST response to obliquity forcing is controlled by the annual-mean insolation anomaly. When obliquity is high, the high latitudes receive significantly more insolation in the summertime, while the tropics receive less. Though in winter the entire hemisphere receives less sunshine when obliquity is high, the summertime forcing is much larger than that of winter, so that the annual-mean forcing is dominated by the summertime signal. Hovmuller plots of zonal-mean SST for each of the other seasons (not shown), reveal a nearly identical pattern to that of fig 4A, confirming that the mixed layer ocean has enough memory of the large summertime forcing in the non-summer seasons that the SST response follows the summertime forcing throughout the year. The dashed line of fig 4B summarizes this relationship between obliquity and the extratropical meridional SST gradient: When obliquity is high (low), the gradient is weakened (strengthened).

Fig 5A shows a Hovmuller diagram of the precessional component of NH zonal-mean SST variability. The strongest signals are seen equatorward of about 50°N, with the anomalies becoming larger about 80,000-140,000 yrs before present, when the eccentricity of the earth's orbit was the greatest of the past 165,000 yrs. These signals reach their maximum value when perihelion occurs in mid Fall, and can be understood as a lagged thermodynamic response to precessional forcing. Just as SSTs reach their

13

maximum values two to three months after the summer solstice in the context of the present-day seasonal cycle, these anomalies reach their maximum values in our simulation when perihelion occurs about two to three months prior to the midpoint of the winter season. This explains why the precessional component of the October-mean insolation anomaly at 40°N (fig 5B, orange line) is nearly perfectly in phase with the precessional component of subtropical wintertime SST variability. The relative strength of the precessional signal equatorward of 50°N (owing largely to the fact that the magnitude of the precessional forcing itself increases equatorward) means these latitudes dominate precessional variations in the extratropical meridional SST gradient. A comparison of fig 5A to the dashed line of fig 5B shows the precessional variations in the extratropical meridional SST gradient are closely in phase with precessional variations in subtropical SST.

The causal relationship between the meridional SST gradient and the orbital NAM pattern is suggested by an examination of figs 4B and 5B; both the obliquity and precession components of the meridional SST gradient are nearly perfectly in phase with their respective components of the orbital NAM.   The direction of causality between the SST gradient and the NAM is somewhat ambiguous because the NAM also gives rise to a meridional surface temperature gradient via compressional heating and cooling in the zonally symmetric vertical motion associated with it; however, the SST anomalies seen in figs 4A and 5A are very consistent with a direct thermodynamic response to orbital forcing. Moreover the wintertime SST response to orbital forcing behaves very similarly to the SST response in other seasons (not shown), when dynamical processes are much

14

weaker and the direct thermodynamic response is sure to dominate. The high likelihood

that the SST anomalies of figs 4A and 5A mainly reflect a direct thermodynamic

response to orbital forcing implies that fluctuations in the extratropical meridional SST

gradient are forcing orbital NAM variability, rather than the other way around.

6. Impacts of orbital NAM variability

Significant SAT variability is associated with the NAM, as indicated by the projection of

internal SAT anomalies onto the internal NAM time series (fig 6C). The stronger surface

westerlies implied by the SLP pattern of fig 2G advect warm marine air over cold

continents, and cold continental air over warm oceans. This creates a zonally-asymmetric

SAT pattern, with warm SATs over mid to high latitude continents, and cold SATs over

mid to high latitude oceans. The anomalies are particularly large over northern Europe,

Canada, the Greenland Sea, and the northern N. Pacific.   This is very similar to the SAT

pattern associated with the positive phase of the real atmosphere's NAM (e.g. Hurrell

1995, Thompson and Wallace 2000). These authors also demonstrated that the SAT

anomalies associated with the observed NAM result from advection of warm and cold air

masses by the NAM's anomalous circulation, as described above.

A somewhat similar pattern to fig 6C emerges when orbital SATs are projected onto the

orbital NAM (fig 6A), with warm temperatures over northern Europe and Canada, and

cold temperatures over the Greenland Sea and northern N. Pacific. However, this pattern

is difficult to interpret definitively because it contains SAT anomalies from two sources:

(1) those generated by the circulation anomalies associated with the orbital NAM, as in

the unforced case, and (2) those related to the SST anomalies responsible for exciting the orbital NAM (figs 4 and 5). The latter result from the direct thermodynamic response to orbital forcing, as described in section 4. Since they are related to the mechanism forcing the orbital NAM, they are highly correlated with the orbital NAM index. However, they obviously cannot be interpreted as an impact of the orbital NAM.

To clarify this issue, we removed the zonal-mean variability from the orbital SAT time series and re-projected the zonally-asymmetric orbital SAT variability onto the orbital NAM time series (fig 6B). This allow us to focus more on the SAT impact of the orbital NAM because SAT anomalies resulting from variability in the surface westerlies across the zonally-asymmetric NH land-ocean configuration are more strongly reflected in the zonally-asymmetric component of orbital SAT variability, while SAT anomalies resulting directly from the zonally-symmetric orbital forcing are more strongly reflected in the zonally-symmetric component. The overwhelming similarity between figs 6B and C suggests this decomposition worked: Since the pattern in fig 6C can be thought of as an impact of the internal NAM, the fact that the pattern in fig 6B is nearly identical to it suggests the zonally-asymmetric component of orbital SAT variability can be understood as an impact of the orbital NAM.

Over North America and Eurasia poleward of about 45°N, the zonally-symmetric SAT pattern of fig 6B accounts for most of the total orbital SAT variability seen in fig 6A. In these regions, simulated continental wintertime SAT variations traceable to orbital forcing are therefore determined mainly by the orbital forcing of the atmospheric

circulation, rather than a local response to radiative forcing.   We return to this point when we discuss the paleoclimate implications of our study in section 7.

7. Rules of thumb

Lacking the observed variation in ice volume over the past 165,000 yrs, our simulation likely differs in significant ways from the actual climate variations during this period, particularly at times when the ice sheet distribution differed significantly from the present. However, our idealized experiment gives useful rules of thumb that can be used to interpret the actual paleoclimate record and understand past controls on the NAM:

 (1) Difference between the summer and winter response of the NH climate. During summertime, the circulation response can be understand in terms of a simple local thermodynamic response to orbital forcing; a positive insolation anomaly warms the continents more than the oceans, which leads to low SLP over continents and high SLP over the oceans. In wintertime, on the other hand, the NH response to orbital forcing includes not only a passive thermodynamic response, but also a dynamic response that resembles the dominant mode of internal atmospheric variability. The direct wintertime thermodynamic response to orbital forcing gives rise to variations in the NH extratropical meridional SST gradient. Consistent with the mechanisms outlined in Robinson (2000) and Kushnir et al. (2003), the changes in the midlatitude surface temperature gradient are associated with changes in the tropospheric zonal flow that project onto the signature of the NAM. The dominance of the NAM in internal wintertime variability, and its weakness in summer, can be traced to the relative strength of synoptic-scale eddy activity in winter.

(2) Importance of the extratropical meridional SST gradient during winter. The tight relationship between orbital variations in this quantity and the wintertime circulation suggests it may be particularly useful for understanding past NH wintertime climate variability. Paleoclimate proxies of anomalies in this gradient, whether they arise from orbital forcing or for other reasons, may provide information about past variations in the wintertime circulation and climate.

(3) Seasonal lags between forcing and response. Examining the climate response to continuously varying orbital forcing forces one to confront seasonal lags between forcing and response. Because of the thermal inertia of the ocean, the phasing of the primary mode of the orbital wintertime circulation variability is controlled by insolation anomalies in other seasons: The obliquity component phasing is controlled by annual-mean obliquity forcing, which is dominated by the summertime obliquity signal, while the phasing of the precessional component is controlled by the fall precessional signal. This information would have been overlooked if we had approached this problem by simply taking snapshots of the simulated climate response to orbital forcing at different moments in the past, as is often done in paleoclimate modeling. The design of our experiment and the results we obtained from it also underscores the possibility that any seasonal climate signal revealed in a paleoclimate proxy is not necessarily related to insolation anomalies in that same season, as is often assumed to be the case.

8. Implications

The variability simulated in our model may correspond to actual climate variations during periods of the past 165,000 yrs when the ice sheet distribution resembled that of the present-day. This condition is met during the Holocene, extending approximately 11,000 yrs before present. An examination of the time series of the orbital NAM (black curve, fig 2F) reveals the orbital forcing did not cause large NAM-like fluctuations. This apparently weak response during the Holocene arises largely because of destructive interference between the obliquity and precessional components of the time series (compare the solid black curves of figs 4B and 5B). The insolation in mid Fall due to precession was greater than normal during the Holocene, reaching a maximum when perihelion occurred in October approximately 6,000 yrs ago. This strengthened the extratropical wintertime meridional SST gradient. Obliquity, on the other hand, was relatively high during this period, weakening the extratropical wintertime meridional SST gradient.   This partially counteracted the precessional forcing and made for only relatively small perturbations to the wintertime circulation: We created a combined orbital and internal NAM index based on the raw model time series over the past 11,000 yrs by taking the difference in DJF zonal mean pressure between 38°N and the North Pole. In this time series (not shown), the orbital signals are barely visible, being dominated by the internal variability. We therefore predict relatively small perturbations to the NAM due to orbital forcing during the Holocene compared to levels of variability generated internally by the atmosphere.

The ice sheet distribution also resembled that of the present-day during the last interglacial, or Eemian period, which lasted from approximately 130,000 to 110,000 yrs before present. In contrast to the Holocene, the orbital NAM reached its maximum value of the entire model time series at about this time (fig 2F, black curve), peaking about 120,000 yrs before present. This is mainly because perihelion occurred in NH Fall then, and high eccentricity at this time amplified the precessional forcing (fig 5B). (Fig 4 shows that obliquity was near average at this time, so that obliquity forcing contributed little to the Eemian maximum in the orbital NAM.) This may explain why paleoclimate proxy records indicate winters in Europe during the mid-Eemian were significantly warmer than the present-day (Zagwijm 1996; Aalbersberg and Litt 1998, Klotz et al. 2003). A high NAM index at this time would have increased advection of warm maritime air over the European continent, increasing temperatures there, as in fig 6.

In fact, a time series of simulated orbital SAT averaged over the European continent reaches its maximum of the entire simulation at the midpoint of the Eemian, approximately 120,000 yrs ago (fig 7, solid black curve). The SAT in this continental area might be expected to equilibrate quickly to direct orbital forcing and would therefore be in phase with DJF insolation anomalies if SAT simply responded thermodynamically to orbital forcing. This is the case in summer: JJA insolation anomalies over Europe are nearly perfectly in phase with JJA SATs (not shown). However, it is clear from fig 7 that DJF insolation anomalies averaged over the latitudes of Europe are not in phase with SAT. Instead, there is a nearly perfect in-phase relationship between European SAT and the orbital NAM. The ~1.2°C simulated warming over Europe 120,000 yrs ago relative

to the present can account for a significant fraction of the roughly 2°C wintertime warming inferred from various paleoclimate proxy data (Zagwijm 1996, Klotz et al. 2003). This comparison must not be taken too literally, of course, as the model result represents a continent-wide average, while the proxy data are representative of local conditions and feedbacks completely unresolved by this coarse resolution model. Still, the simulated orbital SAT signal is large enough to suggest that wintertime European temperature fluctuations during the Eemian are controlled at least in part by a NAM-like circulation response to orbital forcing. The raw time series of European SAT (light grey curve in fig 7) serves as a reminder that some warming could also be explained by internal NAM variability; the internal variability in the SAT time series—well-correlated with the internal NAM—is comparable in magnitude to its orbital counterpart.

Finally, we note that several studies have identified NAM-like patterns dominating the NH wintertime atmosphere response to other types of external forcings, such as increasing greenhouse gases and changes in solar irradiance (Shindell et al. 1999; Fyfe et al. 1999; Gillett et al. 2002; Shindell et al. 2001). Therefore our study adds to the growing body of evidence that the NAM-like patterns are excited by external forcings with a wide variety of spatial structures and time scales.

REFERENCES

Aalsbersberg, G., and T. Litt, 1998: Multiproxy climate reconstructions for the Eemian and early Weichselian. *J. Quat. Sci.,* **13**, 367-390.

Berger, A., 1992: Orbital variations and insolation database (contribution 92-007, NOAA/NGDC, Boulder, USA)

Clement, A.C., R. Seager, and M.A. Cane, 1999: Orbital controls on the El Niño/Southern Oscillation and the tropical climate. *Paleoceanography*, **14**, 441–456.

Felis, T., et al. 2004: Increased seasonality in Middle East temperatures during the last interglacial period. *Nature*, **429**, 164-168.

Fyfe, J.C., G.J. Boer, and G.M. Flato. 1999: The Arctic and Antarctic Oscillations and their Projected Changes Under Global Warming. *Geophys. Res. Lett.,* **26**, 1601-1604.

Gillett, N.P., et al., 2002: How linear is the Arctic Oscillation response to greenhouse gases? *J. Geophys. Res.,* **107**, 4022-4028, 10.1029/2001JD000589

Hartmann, D. L., and F. Lo, 1998: Wave-driven zonal flow vacillation in the Southern Hemisphere. *J. Atmos. Sci.,* **55**, 1303-1315.

Hays, J.D., J. Imbrie, N.J. Shackleton, 1976: Variations in the Earth's orbit: Pacemaker of the Ice Ages. *Science*, **194**, 1121-1132.

Hurrell, J. W., 1995: Decadal trends in the North Atlantic Oscillation: Regional temperatures and precipitation. *Science*, **269**, 676-679.

Hurrell, J.W., Y. Kushnir, M. Visbeck, and G. Ottersen, 2003: An Overview of the North Atlantic Oscillation, in *The North Atlantic Oscillation: Climate Significance and*

Environmental Impact, J.W. Hurrell, Y. Kushnir, G. Ottersen, M. Visbeck, Eds., Geophysical Monograph Series, **134**, 1-35.

Imbrie, J. et al., 1984: The orbital theory of Pleistocene climate: support from a revised chronology of the marine d18O record, in A.L. Berger, J. Imbrie, J. Hays, G. Kukla and B. Saltzman (Eds), *Milankovitch and Climate, Part 1*. D. Riedel, Hingham, pp. 269-305.

Jackson C., and A.J. Broccoli, 2003: Orbital forcing of Arctic climate: Mechanisms of climate response and implications for continental glaciation, *Clim. Dyn.*. 21:539-557.

Karoly, D. J., 1990: The role of transient eddies in low-frequency zonal variations of the Southern Hemisphere circulation. *Tellus*, **42A**, 41-50.

Kidson, J. W., 1988: Indices of the southern hemisphere zonal wind. *J. Climate,* **1**, 183-194.

Klotz, S., J. Guiot, and V. Mosbrugger, 2003: Continental European Eemian and early Wurmian climate evolution: comparing signals using different quantitative reconstruction approaches based on pollen. *Glob. Planet. Change*, **36**, 277-294.

Kushnir, Y., W. A. Robinson, I. Blade, N. M. J. Hall, S. Peng and R. Sutton, 2002: Atmospheric GCM response to extratropical SST anomalies: Synthesis and evaluation. *J. Climate*, **15**: 2233-2256.

Limpasuvan, V., and D.L. Hartmann, 2000: Wave-Maintained Annular Modes of Climate Variability. *J. Climate*, **13**, 4414-4429.

Lorenz, D.J., and D.L. Hartmann, 2003: Eddy-Zonal flow feedback in the Northern Hemisphere Winter. *J. Climate*, **16**, 1212-1227.

Philander, G.S., 1990: *El Niño, La Niña, and the Southern Oscillation*, Academic   Press.

Robinson, W. A., 2000: A Baroclinic Mechanism for the Eddy Feedback on the Zonal Index, *J. Atmos. Sci*., **57**, 415-422.

Shindell, D.T., R.L. Miller, G.A. Schmidt, and L. Pandolfo, 1999: Simulation of recent northern winter climate trends by greenhouse-gas forcing. *Nature,* **399**, 452-455.

Shindell, D.T., G.A. Schmidt, M.E. Mann, D. Rind, and A. Waple, 2001: Solar forcing of regional climate change during the Maunder Minimum. *Science* **294**, 2149-2152.

Thompson, D.W.J., and J.M. Wallace, 2000: Annular modes in the extratropical circulation. Part I: Month-to-month variability. *J. Climate*, **13**, 1000-1016.

Thompson, D.W.J., and J.M. Wallace, 2001: Regional Climate Impacts of the Northern Hemisphere Annular Mode. *Science*, **293**, 85-89.

Zagwijn, W.H. 1996: An analysis of Eemian climate in western and central Europe. *Quat. Sci. Rev.,* **15**, 451-469.

Figure Captions

Figure 1. An example of the least-squares fitting procedure used to separate raw model time series into orbital and internal variability components.   A. the raw model time series of SLP at a grid point near the Azores in the central North Atlantic (42°N, 38°W). Orbital periodicities as well as internal variability are clearly visible.   B. the variability in panel A that can be linearly related to orbital forcing, given by the sum of the variability that can be linearly related to obliquity forcing (panel C), and the variability that can be linearly related to precessional forcing (panel D). Panel E is what remains when the orbital variability of panel B is subtracted from the raw model time series in panel A. This is clearly mostly internally-generated variability. The abscissa of each panel spans 165,000 yrs (30 times the actual 5,500 yr length of the model integration) to reflect the forcing acceleration technique described in section 2. Decadal means of the 5,500 yr long model time series were used so that only 550 data points are plotted in each panel.

Figure 2. The patterns of the first EOFs (A,C,E,G), and associated time series (B,D,F,G, black lines) for orbital and internal variability components of simulated SLP poleward of 26.7°N. (A,B) JJA orbital variability. The pattern accounts for 96% of the orbital variance. (C,D) JJA internal variability. This pattern accounts for 36% of the internal variance. (E,F) DJF orbital variability. This pattern accounts for 80% of the variance. (G,H) DJF internal variability. This pattern accounts for 61% of the variance. When the EOF analysis is performed separately on the obliquity and precession components of the JJA (DJF) orbital variability, the patterns closely resemble each other and those of panel A (E), so that panel A (E) summarizes the main mode of SLP variability for both types of

orbital forcings. JJA and DJF decadal means of the 5,500 yr long model time series were used for this analysis, so that only 550 data points are plotted in panels B, D, F, and H. Also shown with orange lines are the incoming solar radiation anomalies at 40°N resulting from variations in the earth's orbit, normalized by their standard deviation, for June (panel B) and December (panel F). The phasing of these curves is representative of the phasing of the orbital forcing over the entire NH extratropics because both their obliquity and precessional components are in phase with the orbital forcing elsewhere in the NH extratropics, as implied by the discussion of the character of the orbital forcing given in section 2. The abscissas of panels B, D, F, and H spans 165,000 yrs (30 times the actual 5,500 yr length of the model integration) to reflect the forcing acceleration technique described in section 2.

Figure 3. The vertical structure of the DJF zonal-mean zonal wind ([U]) anomalies accompanying the primary modes of SLP orbital and internal variability. Units in all panels are cm/sec. A. Regression of the orbital component of [U] onto the EOF time series shown in fig 2F (black curve). B. Regression of the internal variability component of [U] onto the EOF time series shown in fig 2H.

Figure 4. Summary of NH wintertime relationship between zonal-mean SST and the primary mode of SLP variability for anomalies related to obliquity variations. A. Hovmuller diagram of the obliquity component of zonal-mean DJF SST (°C) in the NH. Also noted on this panel are times when obliquity is anomalously high and low. B. Normalized time series of the obliquity component of the NH extratropical zonal-mean

DJF SST gradient (dashed line), defined as the difference in zonal-mean DJF SST between 38°N and 74°N. Shown as a solid line in panel B is the obliquity component of the time series associated with the first EOF of orbital DJF SLP variability (figure 2F). This time series has been multiplied by -1 to avoid visual interference with the zonal-mean SST gradient time series.

Figure 5.   As in figure 4, except for anomalies related to the precession of earth's spin axis. Also shown in panel B with a solid orange line is the normalized time series of the precessional component of October-mean orbital insolation anomalies at 40°N.

Figure 6. A. Regression of orbital DJF SAT (°C) variability onto the time series associated with the first EOF of orbital DJF SLP variability (figure 2F, black curve). B. Regression of the zonally asymmetric component of orbital DJF SAT variability onto the time series associated with the first EOF of orbital DJF SLP variability. Zonally asymmetric SAT variations were calculated by first removing the zonal-mean SAT variation. B. Regression of internal DJF SAT variability onto the time series associated with the first EOF of internal DJF SLP variability (figure 2H).

Figure 7. Time series of: (1) orbital DJF SAT (°C) averaged over the model's European continent, which includes all land areas from 36°N to 77°N, and from 4°W to 56°E. (2) the DJF incoming insolation due to Milankovitch forcing averaged over these same latitudes. This time series has been normalized by its standard deviation. (3) the primary mode of orbital SLP variability (same as the black curve of fig 2F).   The raw 30-yr-

mean DJF SAT anomaly time series averaged over the model's European continent is

also shown in light grey.

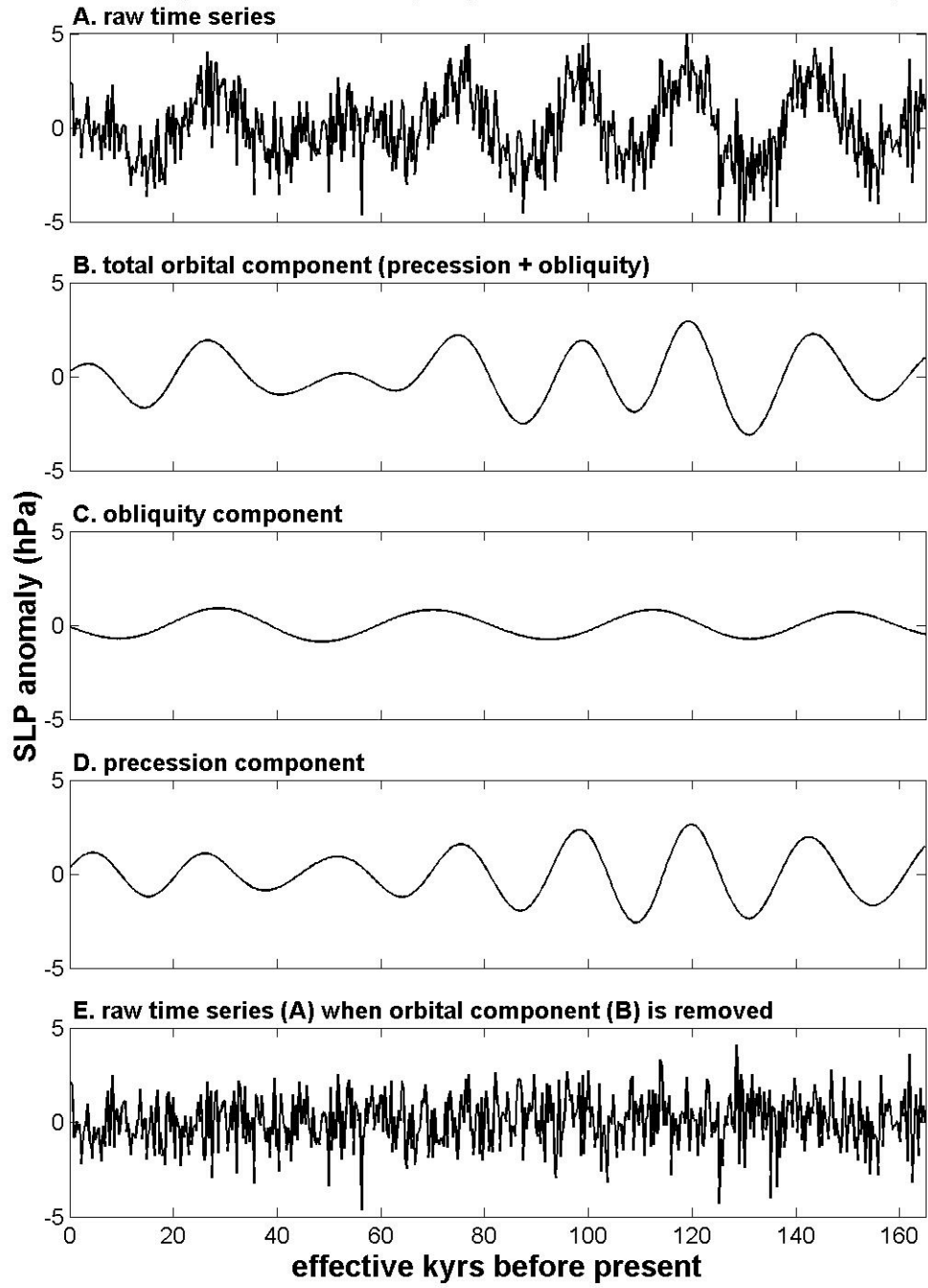Figure 1

EOF analysis of orbital and internal SLP variability

insolation-40°N

normalized amplitude

effective kyrs before present

Figure 2

[U] projection onto SLP 1st EOF

Figure 3

A. zonal mean SST vs time

OBLIQUITY

B. time series

- - - zonal mean SST gradient
— 1st SLP EOF (multiplied by -1)

effective kyrs before present

Figure 4

A. zonal mean SST vs time

PRECESSION

B. time series

October-mean solar forcing, 40°N
zonal mean SST gradient
1st SLP EOF (multiplied by -1)

effective kyrs before present
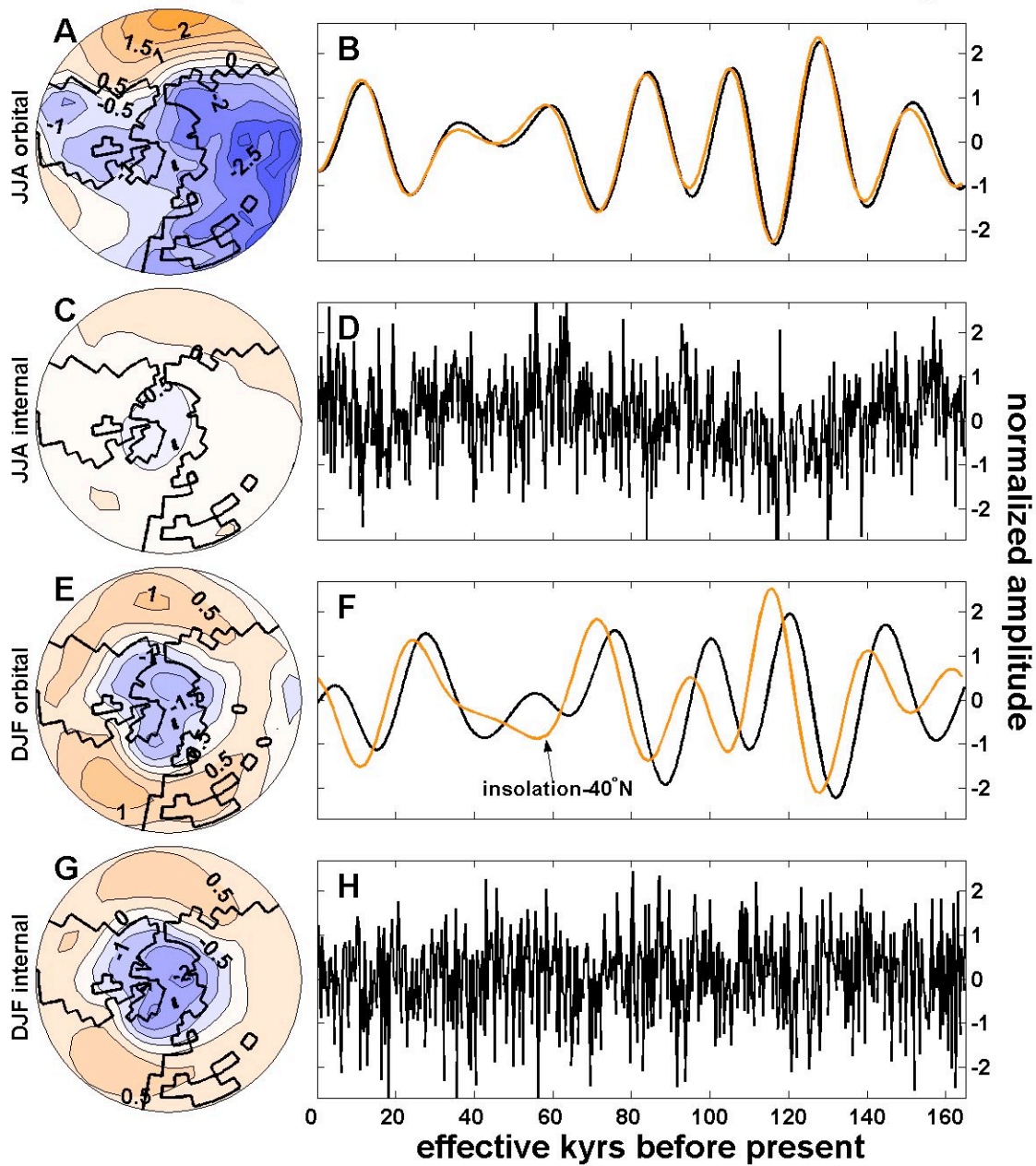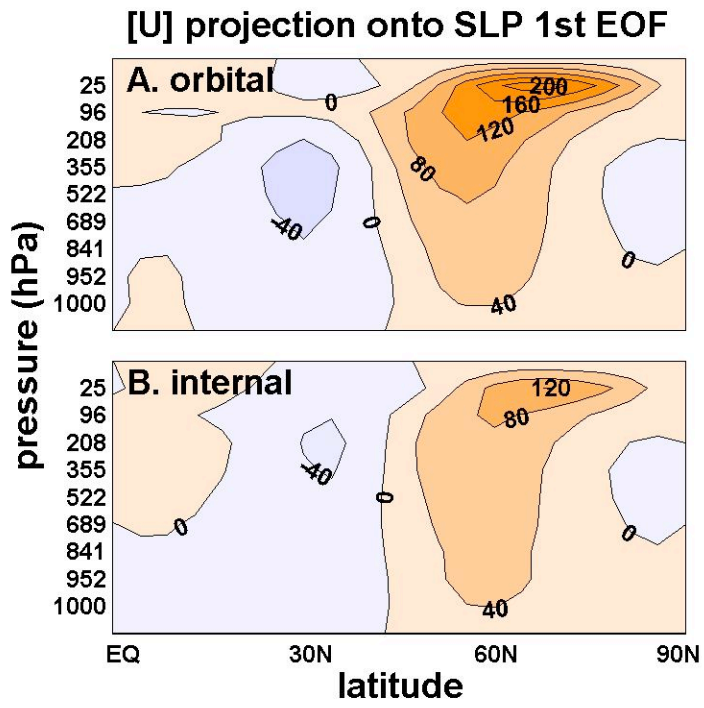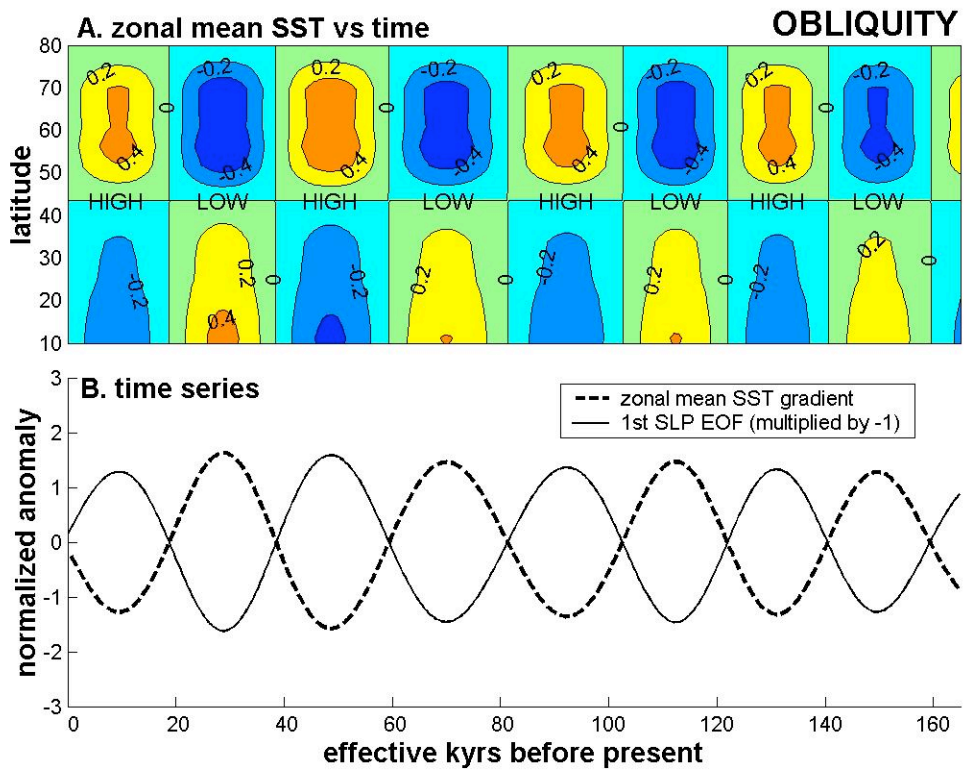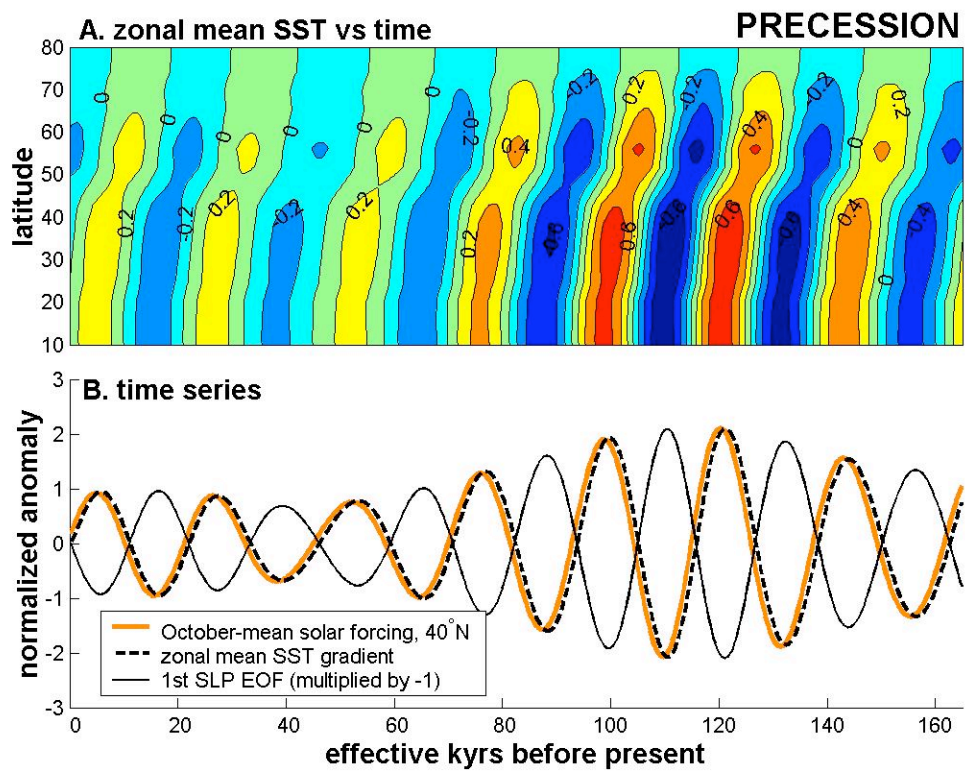
Figure 5

SAT variability projected onto SLP 1st EOF

orbital   orbital-zonal mean removed   internal

Figure 6

Figure 7